International Symposium
On Turbulence and Shear Flow
Phenomena (TSFP-9)
June 30 - July 3, 2015 *Melbourne, Australia*

ON THE ENTRAINMENT OF ACCELERATING SHEAR LAYERS

Giuseppe A. Rosi* **and David E. Rival**
Department of Mechanical and Materials Engineering
McLaughlin Hall, Queen's University
Kingston, ON, Canada, K71 3N6,
*g.rosi@queensu.ca

BACKGROUND

Entrainment, which refers to the assimilation process of low-vorticity fluid into high-vorticity fluid along a turbulent non-turbulent interface (TNTI), is a phenomenon that occurs wherever a shear layer is present. Needless to say, this makes entrainment a ubiquitous process. The exterior of jets, the intermediate interface of mixing layers, the edge of turbulent boundary layers and the periphery of isolated vortices all exhibit some form of entrainment (Dimotakis, 1986; Shadden *et al.*, 2007; Wolf *et al.*, 2013; Chauhan *et al.*, 2014). Given the universality of these canonical flows, one must not look far to find entrainment in both engineering and nature.

In a seminal paper by Corrsin & Kistler (1955), it was proposed that the TNTI possessed a finite thickness, across which sharp spatial gradients in enstrophy, velocity and Reynolds stresses should be observed. Due to technological limitations, the ability to verify this proposal have been impossible until recently. The advent of velocimetry measurement techniques have allowed for the spatially-resolved, conditional averaging of the cross-flow gradients relative to the TNTI. This in turn has shown the existence of the sharp spatial gradient along the TNTI's lower envelope. Sharp gradients across the TNTI have now been repeatedly observed in jets (Wolf *et al.*, 2013; Mistry & Dawson, 2014), in canonical turbulent boundary layers (Chauhan *et al.*, 2014) and in stratified flows (Krug *et al.*, 2013). Current studies on entrainment have shown that regardless of flow configuration, the entrainment of irrotational fluid into the turbulent region follows a multi-step process: (i) an induced inflow within the turbulent region draws irrotational fluid towards it; (ii) irrotational fluid is engulfed within interfacial areas of the TNTI generated by large-scale eddies; (iii) small-scale eddies transport kinetic energy from the turbulent region to the engulfed fluid; and finally (iv) passive scalars are mixed via molecular motions (Phillip & Marusic, 2012; Mistry & Dawson, 2014).

The current methodology used to investigate entrainment exhibits limitations. The primary concern is the use of conditional averaging, which is suitable for stationary, ergodic flows. In such flows, the low-vorticity region and the high-vorticity region have a negligible time derivative, and the flow exhibits self-similarity along some axis. In contrast, unsteady flows are neither stationary nor do they exhibit self-similarity, thereby making them unsuitable for conditional averaging. For example, contrast the TNTI far downstream of a turbulent jet to that of a starting vortex that forms on the suction side of an accelerating two-dimensional body, as illustrated in Fig. 1. For convenience, a one-dimensional axis s is fixed to the origin of the TNTI and all scalar properties of the flow field (e.g. velocity and vorticity components) are represented by Λ. For the case of a steady jet, the mean time derivative of Λ is zero. Furthermore, the mean spatial derivative of Λ along s is zero if the radial axis is normalized by the jet's half radius. This thereby permits conditional averaging to be performed at different locations along the TNTI (points A and B) and at different times (A and B with C). However, such is not the case for the TNTI that forms behind the accelerating plate. It is unclear that the conditional averaging of the TNTI at a single time instance would produce a meaningful result as it is no longer necessary for the TNTI to be spatially similar along s. Furthermore, it is almost certain that the conditional averaging of the TNTI from different instances in time would result in a nonsensical result as the mean contour of the TNTI develops with time. The unsuitability of conditional averaging for non-ergodic flows underscores a need for alternate methods in studying the entrainment dynamics of accelerating-flow cases. Furthermore, conditional averaging is inherently weak in studying issues of transport as it is devoid of any temporal information. The heavy reliance on conditional averaging in studying entrainment may stem from the traditional acquisition of data in an Eulerian framework using existing probes such as hotwires or Particle Image Velocimetry (PIV). The flow history of fluid as it is transported across the TNTI, which requires data acquisition to be performed in a Lagrangian framework, offers new insight into entrainment dynamics. New measurement techniques to acquire Lagrangian data, such as "Shake-The-Box" Tomographic Particle Tracking Ve-

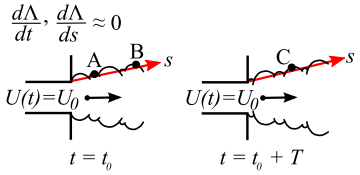

(a) ergodic flow (e.g. jet)

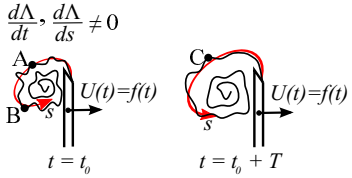

(b) accelerating flow (e.g. plate)

Figure 1. Schematics of entrainment in an ergodic flow (a) and an accelerating flow (b). Ergodic flows allow for the conditional averaging of the TNTI at different locations (A and B) and at different time instances (A, B and C). In contrast, accelerating flows do not lend themselves to conditional averaging since different locations along the TNTI are not necessarily similar and different time instances are not comparable.

locimetry (Tomo-PTV) described in Schanz *et al.* (2013, 2014), as well as with the development of methods to extract meaningful properties of the flow from such data (Rosi *et al.*, 2014) have made the Lagrangian framework an increasingly attractive alternative for studying entrainment. Furthermore, the advent of Lagrangian coherent structures offers a frame-independent method for identifying the TNTI (Peacock & Haller, 2013).

The Lagrangian framework offers the experimentalist a new alternative for studying entrainment that both lends itself towards the study of accelerating-flow cases and towards understanding fluid transport across the TNTI. Thus, the current study works towards the development of an alternative method in studying entrainment for accelerating-flow cases through a Lagrangian framework. As a first step towards this goal, the current study presents a method for quantifying entrainment across an accelerating shear layer. A plate towed normal to its path at a constant rate of acceleration is used as a case study. Similar to Shadden *et al.* (2006), the method for calculating entrained mass uses the forward finite-time Lyapunov exponent (FTLE) field within the wake of the plate to determine total mass of rotational region, and measurements of the shear layer at the plate's edge to determine the vorticity-containing mass fed to the rotational region. By taking the difference of these two masses, the entrained mass is thus determined. The shear-layer and FTLE measurements are first considered separately, and then jointly when the method for calculating entrained mass is presented.

APPARATUS & METHODS

2D-PTV measurements were acquired behind an impulsively started, 3mm-thick, knife-edged plate with a chord of $c = 50$mm that was towed through a free-surface water channel at a 90° angle-of-attack. Fig. 2(a) presents a schematic of the towed-plate experiment, while Fig. 2(b) presents various experimentally pertinent lengths, including plate-tip gaps, aspect ratio, channel dimensions, field-of-view (FOV) area and laser-sheet thickness. The plate was accelerated constantly at 0.1m/s^2 and 0.4m/s^2, which will be referred to hereafter as the slow- and fast-acceleration cases, respectively. The towing motion produced a symmetric vortex pair on the suction side of the plate. PTV- and PIV-amenable images of a single vortex were acquired along the plate's midspan, within a $1.2c$ by $1.2c$ FOV, and a $0.6c$ by $0.6c$ FOV, respectively. The PTV measurements were used to quantify the total mass of the vortex, while the PIV measurements were used to determine vorticity-containing mass. To ensure that an equal number of images were acquired between test cases, the slow- and fast-acceleration cases were measured using frame rates of 500Hz and 1000Hz, respectively. 100 runs of PIV and PTV data were acquired for each acceleration case. The PIV data was phase averaged, while the PTV data was compiled into a single data set to improve spatial density. Images were then imported into DaVis 8.2.0 for analysis, and resulting data were than exported to MATLAB R2012a for post-processing. For the PTV data, vorticity fields and FTLE fields were than calculated using a verified unstructured-grid gradient algorithm. Further details of the apparatus and algorithm may be found in Rosi *et al.* (2014).

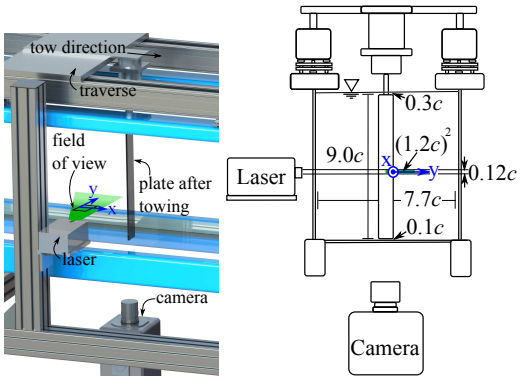

(b) (c)

Figure 2. (a) Schematic of towed-plate apparatus. (b) Upstream view of apparatus with relevant dimensions.

RESULTS

The current section first presents shear-layer measurements to determine the rate at which vorticity-containing mass enters the starting vortex. The forward FTLE field as calculated by the PTV data is then demonstrated to accurately demarcate the vortex from the ambient fluid, thereby acting as a effective tool to calculate the total mass of the vortex. A method developed after Dabiri & Gharib (2004) and Shadden *et al.* (2006) is presented for quantifying entrained mass into the vortex that forms behind the towed plate.

Shear-Layer Measurements

Fig. 3 presents the development of the starting vortex for both acceleration cases at two snapshots of equal towed distances,

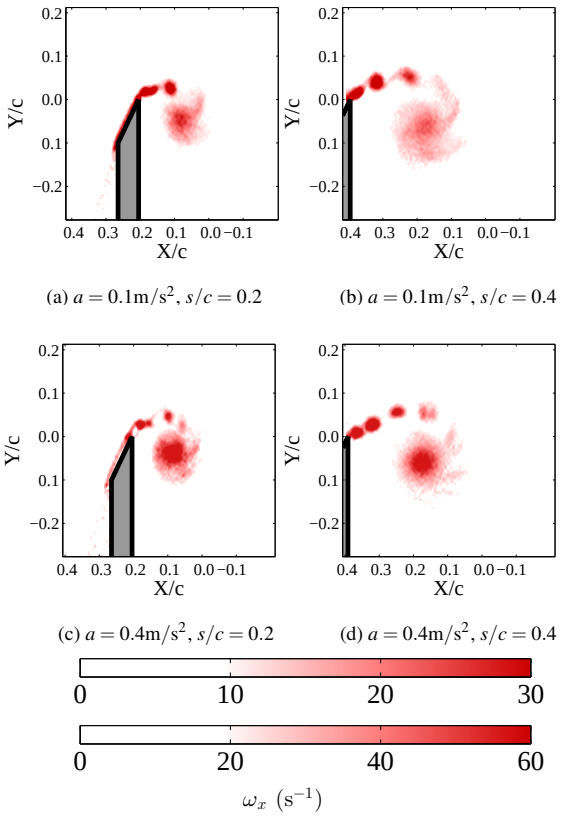

Figure 3. Development of a vortex behind a linearly accelerating plate travelling at two different accelerations. Vorticity is shown in red, and the top and bottom colourbars pertain to the figures in the upper and lower rows, respectively. In spite of travelling at different accelerations, the development of the vortex collapses well with distance travelled by the plate.

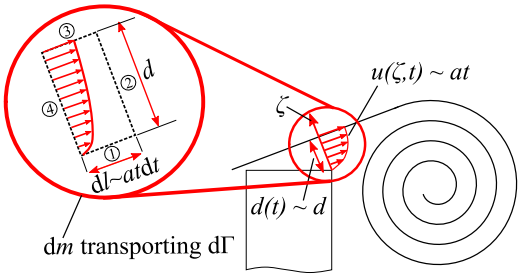

Figure 4. Parameters that dictate vorticity-containing mass of the starting vortex behind a plate traversing at a velocity, at. The starting vortex is fed by a shear layer of thickness, which is assumed to be a constant, d. The velocity profile of the shear layer is $u(\zeta,t)$ and is approximated as the plate velocity, at. The vorticity-containing mass of the starting vortex can be determined by integrating the contributions made by infinitesimal mass units $\mathrm{d}m_\omega$. The spatial dimensions of $\mathrm{d}m_\omega$ are provided in the inset.

s/c. In each image, the plate was towed from left to right, generating a free shear layer that moves from right to left. The vortex and the instabilities that encircle it appear nearly identical between acceleration cases at instances of equal s/c, which suggests that the vorticity-containing mass and the shear-layer structure scale with the distance travelled by the plate regardless of the acceleration. To understand the apparent scaling of vorticity-containing mass with distance travelled by the plate, the current work adapts the derivation found in Wong *et al.* (2013), which equates the vorticity-containing mass of the starting vortex to the mass that passes through the shear layer. Fig. 4 provides a schematic of a starting vortex developing behind a infinitely-wide, flat plate undergoing a linear acceleration. The starting vortex is fed vorticity-containing mass from the shear layer, which has a thickness and velocity profile of $d(t)$ and $u(\zeta,t)$, respectively. Here ζ represents the cross-stream position along the shear layer, while t is time. The vorticity-containing mass per unit span can be determined by integrating the mass transported through the shear layer over the entire timespan of the motion:

$$m_\omega = \rho b \int_0^t \int_0^d u(\zeta,T)\,\mathrm{d}\zeta\,\mathrm{d}t. \tag{1}$$

If the thickness of the shear layer can be assumed constant, and if the velocity across the shear layer can be assumed on the order of the plate velocity, then the vorticity-containing mass (per unit thickness) fed by the shear layer into the vortex can be expressed as:

$$m_\omega \sim \rho d \int_0^t u\,\mathrm{d}t = \rho d s. \tag{2}$$

Here, ρ is the fluid density, d is the thickness of the shear layer, and s is the distance traversed by the plate. Eq. 2 suggests that if the plate traverses some swept distance, then the vorticity-containing mass will be equal regardless of the acceleration rate, which agrees with the vorticity fields shown in Fig. 3. This assumes that the shear-layer thickness (d) is constant. The 2D-PIV measurements are revisited to verify this assumption, from which the shear-layer thickness can be determined as a function of towed distance. The method proposed by Brown & Roshko (1974) is used. The method

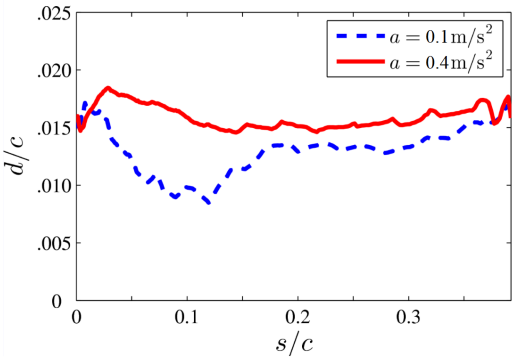

Figure 5. Shear-layer thickness (d/c) as a function of towed distance, s/c. For both accelerations, the thickness is approximately constant.

involves determining the point maximum vorticity on the pressure side of the plate and subsequently evaluating the following expression:

$$d = |\omega_{\mathrm{MAX}}|^{-1} \int_{-\infty}^{\infty} |\omega|\,\mathrm{d}\zeta, \tag{3}$$

where ω is vorticity and ζ, like in Fig. 4, represents the cross-stream axis along the shear layer. For the method described here, ζ is set to pass through the point of maximum vorticity, in the direction normal to the velocity at this point. Shear-layer thickness (d/c) as a function of towed distance (s/c) is plotted for both accelerations in Fig. 5. With the exception of a slight increase and decrease initially exhibited by the fast- and slow-acceleration cases, respectively, the shear-layer thickness is approximately constant. The oscillation in thickness observed at $s/c < 0.1$ for both acceleration cases is attributed to the difficulty in differentiating the starting vortex from the shear layer at the initial portion of the tow. The starting vortex and shear layer are both in close proximity and of equal scale, making their differentiation difficult. In spite of this, a general increasing or decreasing in shear-layer thickness with increasing s/c is not observed. Nor is there any dependence on shear-layer thickness with acceleration. Thus, the results support the assumption of constant shear-layer thickness and in turn that vorticity-containing mass must scale with towed distance, s.

FTLE-Field Measurements

Fig. 6 presents scatter plots of tracked particles in the plate's wake for both linear accelerations. Two towed distances are presented here: $s/c = 0.125$ and $s/c = 0.250$. Particles have been coloured white to red and white to blue according to their vorticity and FTLE values, respectively. The FTLE and vorticity fields have been calculated using pathlines with temporal lengths of 50% that of the vortex's timescale, which is defined as the time required for a particle located along the periphery of vortex to complete a single orbit about the vortex. As the plate traverses from left to right, the high-vorticity region grows in area. In turn, the FTLE separatrix that encircles the high-vorticity region grows. The area the separatrix encircles can be considered as the total mass of the vortex, m_T. This method was also used by Shadden *et al.* (2006) to determine the total mass of a vortex ring.

The FTLE separatrices presented in Fig. 6 are thick and appear with breakages, which in turn makes it difficult to accurately determine the mass of the starting vortex. These issues are

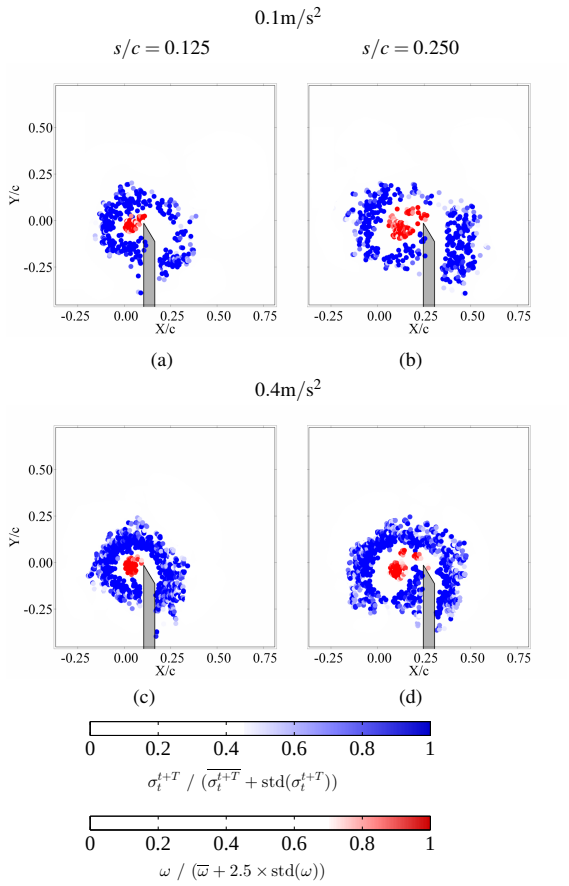

Figure 6. FTLE and vorticity (blue and red, respectively) for a vortical flow generated by the towed plate at two towed distances, $s/c = 0.125$ and 0.250, and travelling at two linear accelerations, $a = 0.1\text{m/s}^2$ and 0.4m/s^2, as indicated by the column headers. The FTLE fields presented here are calculated from pathlines with temporal lengths of 50% that of the vortex's timescale.

likely caused by compilation of several runs into a single data set, since compiling runs increases the noise within the computed FTLE field due to inter-trial intermitencies. To address this, the experiments are currently being repeated using the "Shake-The-Box" Tomographic-PTV evaluation approach described in Schanz *et al.* (2013, 2014). The evaluation approach provides sufficient spatial density to calculate the FTLE within a single run, thereby eliminating the need for run compilation.

Integral Method for Entrained Mass

An integral method for determining entrained mass is presented here. The method relies on LCS identification and is similar to the method used by Dabiri & Gharib (2004) and Shadden *et al.* (2006). The workings of the method are discussed here.

The integral approach is shown schematically in Fig. 7. Vorticity-containing mass (m_ω) is fed into the vortex from the shear layer while irrotational mass (m_ε) is simultaneously entrained into the vortex. The total mass of the vortex is simply $m_T = \rho A_T$, where ρ and A_T represent the fluid density and the planar area of the vortex, while the vorticity-containing mass is determined as $m_\omega = \rho ds$, where d and s are the shear-layer thickness and distance travelled by the plate. The entrained mass (m_ε) is taken as the difference

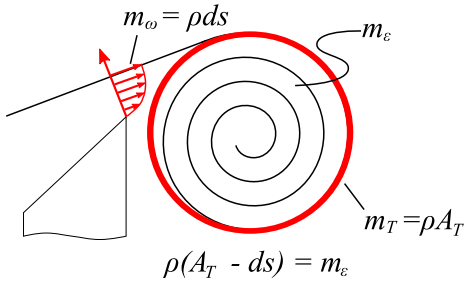

Figure 7. Methodology for calculating entrained mass via the control-volume approach. Entrained mass (m_ε) is evaluated as the difference between vorticity-containing mass (ρds) and the total mass contained by the starting vortex (ρA_T).

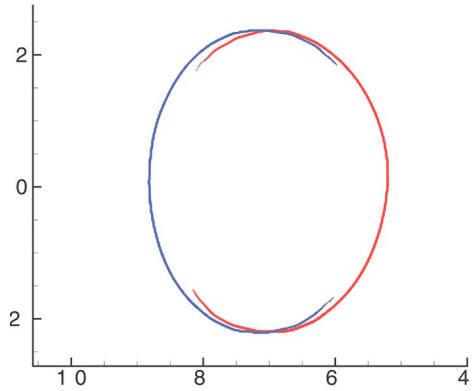

Figure 8. Backward- and forward-FTLE ridges (red and blue, respectively) about the planar area of a vortex ring; from Shadden *et al.* (2006).

between the total vortex mass and the vorticity-containing mass:

$$\rho(A_T - ds) = m_\varepsilon. \tag{4}$$

The method requires accurate measurements of the shear-layer thickness and the total area of the vortex. The shear-layer thickness can be measured directly through planar PIV measurements within a field-of-view on the order of the shear layer. The planar area of the vortex is can be evaluated from the sepratrix that is formed by the FTLE field. Standard PTV evaluation techniques do not produce a sufficiently-defined seperatrix to accurately determine the total mass of the starting vortex. However, given sufficient spatial density within a single run, the FTLE field has been shown to precisely demarcate rotational fluid from ambient fluid, as was done by Shadden *et al.* (2006) for the counter-rotating vortices of a vortex ring, see Fig. 8.

CONCLUSIONS & OUTLOOK

To study the entrainment across an accelerating shear layer, PIV and PTV measurements were performed in the wake of an accelerating plate. The plate was accelerated at two constant rates of acceleration, and towed normal to its path. The PIV measurements demonstrated that the thickness of the shear-layer that forms at the plate edge remains constant with time. The result suggests that the vorticity-containing mass may be represented as ρds, where

ρ is fluid density, d is the shear-layer thickness and s is the distance traversed from the plate. Using an unstructured gradient algorithm described in Rosi *et al.* (2014), FTLE and vorticity fields were calculated directly from the PTV measurements. The FTLE formed a separatrix that divided the starting vortex from the ambient fluid. Thus, the area contained by the separatrix represented the total mass of the starting vortex. However, the thickness of the separatrix, as well as the breakages that appeared along the separatrix's length made it difficult to accurately determine the enclosed area. The poor quality of the separatrix was likely caused by the compilation of all 100 runs into a single data set, since the compilation of runs introduces noise due to inter-trial intermittencies. Given the current quality the separatrix, total mass of the starting vortex was left unmeasured.

To accurately measure the entrainment into the starting vortex, a more precisely defined separatrix must be achieved. Towards this end, new PTV measurements are being acquired using the "Shake-The-Box" Tomographic PTV (TOMO-PTV) evaluation approach described in Schanz *et al.* (2013, 2014). The approach achieves a sufficient spatial density for calculating the FTLE within a single run, and thereby eliminates the need for run compilation. It is expected that these new measurements will result in a precisely defined separatrix from which the total mass of the starting vortex can be determined. Finally, by subtracting the vorticity-containing mass as determined from the shear-layer measurements from the total mass of the starting vortex, the mass entrained across the shear layer can be determined.

REFERENCES

Brown, G. L. & Roshko, A. 1974 On density effects and large structure in turbulent mixing layers. *Journal of Fluid Mechanics* **64** (4), 775–816.

Chauhan, K., Philip, J., de Silva, C. M., Hutchins, N. & Marusic, I. 2014 The turbulent/non-turbulent interface and entrainment in a boundary layer. *Journal of Fluid Mechanics* **742**, 119–151.

Corrsin, S. & Kistler, A. L. 1955 Free-stream boundaries of turbulent flows. Tech. rep. NACA.

Dabiri, J. O. & Gharib, M. 2004 Fluid entrainment in isolated vortex rings. *Journal of Fluid Mechanics* **511**, 311–331.

Dimotakis, P. E. 1986 Two-dimensional shear-layer entrainment. *American Institute of Aeronautics and Astronautics Journal* **24** (11), 1791–1796.

Krug, D., Holzner, M., Lüthi, B., Wolf, M., Kinzelbach, W. & Tsinober, A. 2013 Experimental study of entrainment and interface dynamics in a gravity current. *Experiments in Fluids* **54** (1530).

Mistry, D. & Dawson, J. R. 2014 Experimental invstigation of multi-scale entrainment processes of a turbulent jet. In 17^{th} *International Symposium on Applications of Laser Techniques to Fluid Mechanics*.

Peacock, T. & Haller, G. 2013 Lagrangian coherent structures: The hidden skeleton of fluid flows. *Physics Today* **66** (2), 41–47.

Phillip, J. & Marusic, I. 2012 Large-scale eddies and their roles in entrainment in turbulent jets and wakes. *Physics of Fluids* **48** (055108).

Rosi, G. A., Walker, A. M. & Rival, D. E. 2014 The identification of Lagrangian coherent structures in a nominally two-dimensional shear flow via Lagrangian particle tracking. In 17^{th} *International Symposium on Applications of Laser Techniques to Fluid Mechanics*.

Schanz, D., Schröder, A. & Gesemann, S. 2014 "Shake-The-Box" - a 4D-PTV algorithm: Accurate and ghostless reconstruction of Lagrangian tracks in densely seeded flows. *Proceedings of the* 17^{th} *International Symposium on Applications of Laser Techniques to Fluid Mechanics* .

Schanz, D., Schröder, A., Gesemann, S., Michaelis, D. & Wieneke, B. 2013 "Shake-The-Box": A highly efficient and accurate tomographic particle tracking velocimetry (TOMO-PTV) method using prediction of particle positions. *Proceedings of the 10th International Symposium on Particle Image Velocimetry* .

Shadden, S. C., Dabiri, J. O. & Marsden, J. E. 2006 Lagrangian analysis of fluid transport in empirical vortex ring flows. *Physics of Fluids* **18** (047105), 1–11.

Shadden, S. C., Katija, K., Rosenfeld, M., Marsden, J. E. & Dabiri, J. O. 2007 Transport and stirring induced by vortex formation. *Journal of Fluid Mechanics* **593**, 315–331.

Wolf, M., Holzner, M., Krug, D., Lüthi, B., Kinzelbach, W. & Tsinober, A. 2013 Effects of mean shear on the local turbulent entrainment process. *Journal of Fluid Mechanics* **731**, 95–116.

Wong, J., Kriegseis, J. & Rival, D. E. 2013 An investigation into vortex growth and stabilization for two-dimensional plunging and flapping plates with varying sweep. *Journal of Fluids and Structures* **43**, 231–243.